

Article

Magnetoelectric and Multiferroic Properties of BaTiO₃/NiFe₂O₄/BaTiO₃ Heterostructured Thin Films Grown by Pulsed Laser Deposition Technique

Venkata Sreenivas Puli ^{1,2,3,*}, Dhiren Kumar Pradhan ⁴, Gollapudi Sreenivasulu ⁵, Simhachalam Narendrababu ⁶, Nandiraju Venkata Prasad ⁶, Kalpana Madgula ⁷, Douglas B. Chrisey ² and Ram S. Katiyar ¹

- ¹ Department of Physics, University of Puerto Rico, Puerto Rico, San Juan, PR 110007, USA; rkatiyar@hpcf.upr.edu
- ² Department of Physics & Engineering Physics, Tulane University, New Orleans, LA 70118, USA; dchrisey@tulane.edu
- ³ National Research Council, Washington, DC 20001, USA
- ⁴ Extreme Materials Initiative, Geophysical Laboratory, Carnegie Institution for Science, Washington, DC 20015, USA; dhirenkumar@gmail.com
- ⁵ Department of Materials Science and Engineering, Virginia Tech, Blacksburg, VA 24060, USA; sreeni@vt.edu
- ⁶ Department of Physics, Osmania University, Hyderabad 500007, India; narendraphysics@gmail.com (S.N.B.); nvp1969@rediffmail.com (N.V.P.)
- ⁷ SAS Nanotechnologies LLC, 506 First State Blvd, Wilmington, DE 19804, USA; kalpanasekhar@yahoo.com
- * Correspondence: pvsri123@gmail.com
- † Authors Current Address: National Research Council (NRC) Senior Research Associate, Materials and Manufacturing Directorate, Air Force Research Laboratory, 3005 Hobson Way, Wright Patterson Air Force Base, OH 45433, USA.



Citation: Puli, V.S.; Pradhan, D.K.; Sreenivasulu, G.; Babu, S.N.; Prasad, N.V.; Madgula, K.; Chrisey, D.B.; Katiyar, R.S. Magnetoelectric and Multiferroic Properties of BaTiO₃/NiFe₂O₄/BaTiO₃ Heterostructured Thin Films Grown by Pulsed Laser Deposition Technique. *Crystals* **2021**, *11*, 1192. <https://doi.org/10.3390/cryst11101192>

Academic Editor: Anna Paola Caricato

Received: 31 August 2021
Accepted: 28 September 2021
Published: 30 September 2021

Publisher's Note: MDPI stays neutral with regard to jurisdictional claims in published maps and institutional affiliations.



Copyright: © 2021 by the authors. Licensee MDPI, Basel, Switzerland. This article is an open access article distributed under the terms and conditions of the Creative Commons Attribution (CC BY) license (<https://creativecommons.org/licenses/by/4.0/>).

Abstract: Development of lead-free BaTiO₃/NiFe₂O₄/BaTiO₃ (BTO/NFO/BTO) trilayer structure thin films is significant for the realization of eco-friendly and implantable microelectromechanical systems (MEMS)-based devices. In the present work, we report BTO/NFO/BTO trilayer structure as a representative ferroelectric/ferromagnetic/ferroelectric (FE/FM/FE) system deposited on Pt(111)/TiO₂/SiO₂/Si using Pulsed Laser Deposition (PLD) technique. We report the ferroelectric, magnetic, and ME properties of BTO/NFO/BTO trilayer nanoscale heterostructure having dimensions 140/80/140 nm, at room temperature. High room temperature dielectric constant ~2145 at 100 Hz with low dielectric loss ~0.05 at 1 MHz is observed. Further, the deposited (BTO/NFO/BTO) tri-layered thin films showed magnetoelectric, multiferroic behavior with remanent polarization of 8.63 μCcm⁻² at about 0.25 MV/cm and a reasonably high saturation magnetization of ~16 emu/cm³ at ~10 kOe is witnessed at room temperature. Tri-layered films have shown interesting magnetoelectric (ME) coupling coefficient (α_E) ~54.5 mV/cm Oe at room temperature.

Keywords: polycrystalline; magnetoelectric coupling; multiferroics; Pulsed Laser Deposition; tri-layered films

1. Introduction

Multiferroics (MFs) are those single-phase materials which show the coexistence of at least two or more ferroic ordering, i.e., (ferroelectric (or antiferroelectricity), ferromagnetic (or antiferromagnetism), ferroelastic and ferrotoroidic) at the same temperature and pressure. As most the ferroelectrics are also ferroelastic (stress–strain hysteretic relationships), the multiferroic materials often include three coupled order parameters [1–3]. “Ferroic” materials are provisionally those crystals, when two or more crystal orientation states are in the absence of magnetic field, electric field, and mechanical stress and shift from one state to other state by means of a magnetic field, an electric field, a mechanical stress, or a combination of these [1]. Due to the coexistence of ferroic ordered parameters that

lead to cross coupling between ferroic orders, one ferroic property can be controlled and switched with the conjugate field of the other. Due to their unusual physical properties, MFs materials with magnetoelectric coupling properties have drawn considerable research attention to be utilized in multifunctional devices [2,3]. The fundamental reason is that the coupling between spins and lattices in the crystal of magnetic and ferroelectric and/or structural phase transitions plays a critical role [1]. The coupling between the magnetic and ferroelectric orderings is known as magnetoelectric (ME) coupling which is very important in terms of fundamental physics and device application point of view [3]. ME effect in MFs is observed when the switching of spontaneous magnetization (M_s) by an external electric field and spontaneous polarization (P_s) by an external magnetic field. In either case, these materials exhibit spontaneous deformation, which can also be switched or re-oriented by applied stress (σ). ME materials also assist the conversion among energies stored in magnetic and electric fields. The coupling of these materials can be efficiently used in multifunctional device applications, such as switching devices, novel memory media [low-energy spintronic and magnonic devices], actuators, magnetic sensors and transducers, microwave devices, etc. [2–6].

There are very few room temperature (RT) monophasic MFs that exhibit ME response; however, in single-phase systems (BiFeO_3 and YMnO_3), the magnetoelectric coupling coefficients are very weak at RT [2–6]. Moreover, most of the monophasic multiferroic materials exhibit ferroelectricity and anti-ferromagnetic/ferrimagnetic/ferromagnetic properties at cryogenic temperatures [7,8]. Perovskite structured BiFeO_3 (BFO) is the most extensively studied prototypic ME oxide material. G-type anti-ferromagnetic BFO, with weak ferromagnetic ordering, is the only single-phase material which shows multiferroic phenomena at RT with a relatively high ferroelectric Curie temperature ($T_c \sim 1100$ K) and as well with anti-ferromagnetic Neel temperature ($T_N \sim 640$ K). BFO with rhombohedral ($R3c$) crystal structure favors in the realization of ME coupling by modulating the spin structure. Moreover, weak ferromagnetism in BFO is attributed to canting of the spins [9–11].

Several serious drawbacks of bulk BFO include: its electrical properties, such as high leakage current, small ferroelectric spontaneous polarization, weak magnetization, etc. On the other hand, low electrical resistivity is one among the major drawbacks of pure BFO to measure its multiferroic and ME properties at room temperature. Furthermore, 'Bi' is volatile and difficult to make pure phase BFO in bulk form. Due to these obstacles, several alternative materials were explored for multiferroic ME properties. Bulk lead iron niobate (PFN) is also one among the widely studied single phase ME multiferroic materials, which shows ferroelectric phase transition between 379 and 385 K, with strong anti-ferromagnetic phase transition at around (T_N) ~ 145 – 150 K [12–15]. However, due to lead (Pb) toxicity, Pb based materials are facing restrictions for its applicability in some countries. Few other single phase MF materials/ME materials include AMnO_3 ($A = \text{Y, Bi}$) [YMnO_3 , BiMnO_3], PbBO_3 ($B = \text{Ni, Ti, V}$) [PbNiO_3 , PbTiO_3 , PbVO_3], AlFeO_3 (AF), TbMnO_3 , TbMn_2O_5 , $\text{Ca}_3\text{CoMnO}_6$, $\text{Lu}_2\text{CoMnO}_6$, LuFe_2O_4 , BaNiF_4 , FeTiO_3 and NiTiO_3 , double perovskite $\text{Pb}_2(\text{CoW})\text{O}_6$ [10–21].

In the process of new materials/patterns/nanostructures for aforementioned applications, several composite materials were also explored, consisting of separate piezoelectric and magnetic phases for ME coupling at room temperature [14,15,18–21]. In a two-phase composite of ferroelectric (FE) and piezomagnetic (PM) phases, the external magnetic field induces ME output as a product property. In composite materials, much stronger ME coupling coefficient is realized and is mediated by mechanical stress between ferromagnetic and ferroelectric phases. When a magnetic field is applied to the composite, the ferrite particles elongate or contract along the field direction due to magnetostriction and the resulting strain is transferred to the piezoelectric particles giving rise to an electric polarization [7,8]. However, not all multiferroic materials are essential to generate ME coupling, due to the difficulty of the mutual interaction between ferroic orderings at the same temperature. One drawback with these bulk composites is that they show smaller ME coupling coefficients, due to high leakage current density associated with ferrites. This

problem can be avoided with layered structures with low resistivity, which ultimately leads to the absence of leakage current [7]. Therefore, layered structures can be easily poled, when an electric field is applied, which in turn strengthens the piezoelectric and ME effects respectively [7].

In recent past years, many attempts have been made to overcome the above drawbacks. In addition to intensive efforts in terms of improving the materials preparation and property optimization, various alternative materials and techniques were explored. Thin film growth is an ever growing advanced miniaturization technique or technology with a controlled way of synthesis for producing high quality thin films with improved properties for existing materials by strain engineering and is opening doors for their utilization in device applications. In addition to single-phase BFO and/or chemically doped/substituted BFO thin films, bi-ferroic BiMnO₃ nebulized spray pyrolysis thin films [11,18,19,21–23], few other hexagonal manganite [ErMnO₃ and YMnO₃ (YMO)]-based thin films [24,25], orthorhombically distorted perovskite structured TbMnO₃ thin films [26], Bi₅Ti₃FeO₁₅ thin films [27], and the epitaxial Bi₅Ti₃FeO₁₅-CoFe₂O₄ multiferroic nanostructures were grown by pulsed laser deposition [28] were produced using various deposition techniques, around the globe for their suitability towards magnetoelectric multiferroic applications.

In the present work, we report preparation of multiferroic and magnetoelectric trilayer structure thin films BaTiO₃/NiFe₂O₄/BaTiO₃ (BTO/NFO/BTO) grown on Pt(111)/TiO₂/SiO₂/Si single-crystal substrate using PLD technique. BTO is one of the most studied ferroelectric materials in the perovskite structure family. Perovskite structured materials are on top of the other structures, due to their easy regulation of octahedral distortion, which are beneficial for generating the ME effect. A larger resistive Ni-ferrite (NFO) is cheap and easily available, is useful in obtaining reduced leakage current, and has a much smaller coercive field than CoFe₂O₄. NFO possesses an inverse spinel structure, in which tetrahedral A-sites are occupied by Fe³⁺ ions and octahedral B-sites by Fe³⁺ and Ni²⁺ ions. It exhibits ferrimagnetism that originates from the antiparallel orientation of spins on A- and B-sites. It has been revealed that an increase in temperature and the particle size reduction of the spinel, NFO serves as a material for high-frequency applications in telecommunication field [29].

2. Experimental Procedure

The phase pure ceramic target of BaTiO₃ (BTO) and NiFe₂O₄ (NFO) were prepared by a high-temperature solid-state reaction route using high-purity barium carbonate [BaCO₃; 99.92%, Alfa Aesar, MA, USA], Titanium dioxide [TiO₂; 99.95%, Alfa Aesar, MA, USA] for BTO and oxide precursors of nickel oxide (NiO), and iron oxide (Fe₂O₃) for NFO targets in the required stoichiometry. These ingredients were separately mixed thoroughly using a mortar and pestle for 6 h in ethanol medium. BaTiO₃ (BTO) and NiFe₂O₄ (NFO) targets of one inch diameter were made separately by using the standard method of solid-state synthesis. BTO was calcined at an optimized temperature of 1250 °C for 10 h. Then, the BTO target was sintered at an optimized temperature of 1350 °C for 10 h in air. The NFO powder was calcined at 1350 °C in a high temperature Carbolite box furnace for 10 h. The NFO target was sintered in the furnace at a temperature of 1000 °C for 5 h.

The purity and crystalline structure of sintered targets was observed using X-Ray Diffraction technique using Rigaku; Ultima IV, Japan. Both BTO and NFO target materials were utilized in the ablation process of pulsed laser deposition. These sintered phase pure targets were used for the fabrication of high-purity tri-layered BTO/NFO/BTO thin films. The thin films were grown on Pt(111)/TiO₂/SiO₂/Si. Initially, the PLD chamber was vacuated until a base pressure of 2.7×10^{-9} bar was reached. Then, the oxygen gas was introduced into the chamber to maintain a pressure of 2.7×10^{-4} bar inside the chamber. The BTO and NFO targets were ablated inside the PLD chamber by focusing KrF Excimer Laser ($\lambda = 248$ nm) on the target surface at a laser fluence of 0.8 J cm^{-2} and reiteration rate of 10 Hz. Optimized PLD parameters were listed in Table 1. The average thickness of the deposited film was estimated to be around 360 nm (FE/FM/FE~140/80/140 nm) using stylus

profilo-meter technique (Make: Dektak 150; M/S Veeco) and which is also confirmed using cross-sectional SEM image. The structural peaks of the deposited (BTO/NFO/BTO) trilayer thin films were identified using X-Ray Diffraction instrument (Siemens D5000 diffractometer) operated at 40 kV and at a current equal to 40 mA using Cu-K α rays (wavelength, $\lambda = 1.54 \text{ \AA}$). Raman spectra were measured on films using the micro-Raman spectrometer (Horiba JobinVyon) with a 514 nm excitation laser, an edge filter for Rayleigh line rejection, and a CCD detector. The overall spectral resolution of the system was $\sim 1 \text{ cm}^{-1}$. The laser was focused on the sample to a spot size of $\sim 2 \text{ }\mu\text{m}$ using a $50\times$ objective lens.

Table 1. Pulsed Laser Deposition (PLD) parameters of BTO/NFO/BTO thin films.

PLD Parameters	BTO	NFO
Substrates	Pt/TiO ₂ /SiO ₂ /Si	Pt/TiO ₂ /SiO ₂ /Si
Laser Excimer	KrF Laser	KrF Laser
Target Size	1-inch diameter	1-inch diameter
Target-substrate distance	4.5 cm	4.5 cm
Fluence	0.8 J cm ⁻²	0.8 J cm ⁻²
Laser energy	300–360 mJ	250–350 mJ
Repetition rate of pulsed laser	10 Hz	10 Hz
Ambient gas	O ₂	O ₂
Total pressure of ambient gas (During deposition)	100 mTorr	100 mTorr
Total pressure of ambient gas (During annealing)	300 Torr	300 Torr
Annealing time	30 min	30 min
Deposition temperature	750 °C	650 °C
Growth rate	$\sim 20 \text{ nm min}^{-1}$	$\sim 20 \text{ nm min}^{-1}$

Further, the morphology and surface structure of the grown (BTO/NFO/BTO) trilayered film was characterized by using Field Emission Scanning Electron Microscopy (FE-SEM) (Hitachi S4800). The elemental composition of as-deposited (BTO/NFO/BTO) trilayer thin film was identified using incident Energy Dispersive Spectroscopy (EDX).

Pt top electrodes of area $\sim 10^{-4} \text{ cm}^2$ and thickness $\sim 50 \text{ nm}$ were fabricated utilizing dc sputtering using a metal shadow mask for electrical characterization. The electrical studies of the fabricated (BTO/NFO/BTO) tri-layered thin film-based MIM capacitor (Pt/(BTO/NFO/BTO)/Pt(111)/Ti/SiO₂/Si) were carried out using Keithley-4200 Semiconductor Characterization Unit. The ferroelectric nature of grown (BTO/NFO/BTO) tri-layered thin film was confirmed by ferroelectric P–E loops and were measured using at 4 kHz with a Radiant Precision Multiferroic Materials Analyzer (Radiant Technologies Inc., Albuquerque, NM, USA). The ferromagnetic nature of grown (BTO/NFO/BTO) tri-layered thin film was confirmed by magnetization hysteresis loop (M–H loop) measurements were carried out using a vibrating sample magnetometer (VSM) (Lakeshore 7407), magneto-electric measurement by homemade probe.

3. Results and Discussion

3.1. Structural Study

Figure 1 shows the X-ray diffraction (XRD) patterns of BTO and (BTO/NFO/BTO) trilayer thin films that were deposited on Pt(111)/Ti/SiO₂/Si substrate at room temperature and constant oxygen pressure of $2.7 \times 10^{-4} \text{ bar}$. XRD figure shows typical θ - 2θ scans for the films. XRD patterns reveal BTO peaks corresponding to tetragonal structure with P4mm space group (Figure 1a). Figure 1b displays indexed XRD patterns for heterostructured

thin films consisting of BTO peaks (tetragonal phase) and NFO (cubic inverse spinel with space group $Fd\bar{3}m$). XRD patterns indicates that the BTO/NFO/BTO thin films have a good crystalline and are polycrystalline grown, aligned with respect to their substrate. These XRD patterns are in complete agreement with standard diffraction data with the end members $BaTiO_3$ and $NiFe_2O_4$ [30,31]. This also emphasizes the importance of pulsed laser deposition technique, which can effectively transfer, its stoichiometric compositions in the deposition process.

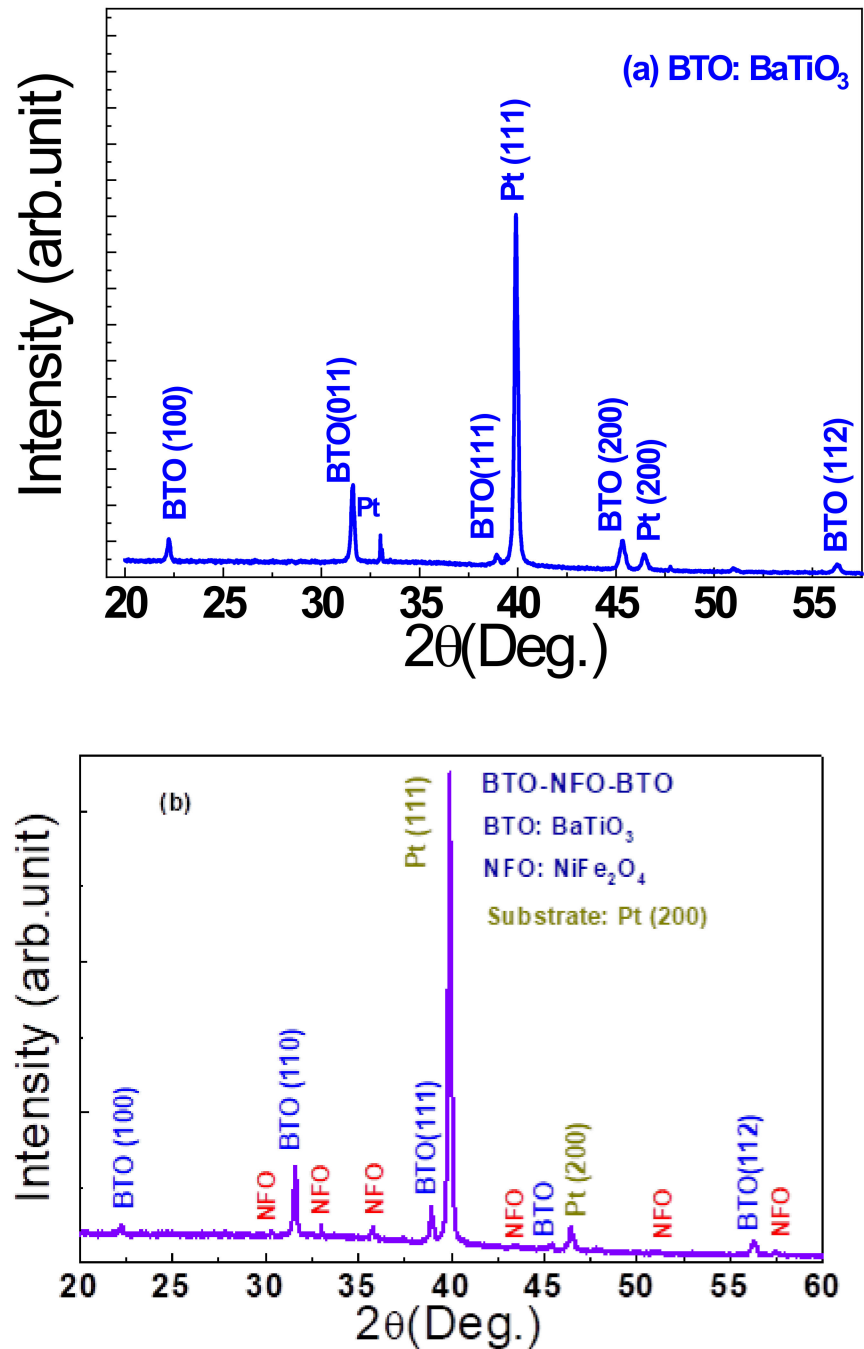


Figure 1. X-ray diffraction pattern of (a) BTO and (b) (BTO/NFO/BTO) tri-layered thin film on substrate Pt/Ti/SiO₂/Si at room temperature.

3.2. Raman Spectroscopy

Raman spectroscopy is a highly sensitive and non-destructive technique of probing the local crystal structure in materials. Raman spectra is an effective tool in probing the short-range disorder in the oxygen octahedral induced by Jahn–Teller distortion, etc., in oxide-based materials [32]. Figure 2 shows the room temperature measured Raman spectra of polycrystalline pure BaTiO₃ and tri-layered BTO/NFO/BTO films. Room-temperature Raman spectra for pure BTO thin films have been characterized by tetragonal phase E₁(TO) ~58 cm⁻¹, A₁(TO₁) ~184 cm⁻¹, B₁/E (TO+LO) ~305 cm⁻¹ and asymmetric broader A₁(TO₂) ~257 cm⁻¹, A₁(TO₃) ~517 cm⁻¹, A₁(LO)/E(LO) ~720 cm⁻¹ modes, respectively. These latter three Raman modes are also present in paraelectric cubic phase, where they are much broader and more symmetrical. The A₁(LO)/E(LO) mode is extremely broad and weak in cubic phase and often considered unique to the tetragonal phase [33,34]. These results are in complete agreement with pure tetragonal ferroelectric phased BTO bulk ceramics [33,34]. Trilayer structure BTO/NFO/BTO films have shown all the corresponding modes to that of Cubic inverse-spinel structure of NFO. As shown in Figure 2b for tri-layered BTO/NFO/BTO films, the BTO-related signals are barely visible and the Raman spectra are closely resembled to that of the pure NFO ferrite phase at room temperature. Our finding seems surprising as BaTiO₃ forms the top layer of the tri-layered films, however from the experimental observation; it can be explained taking into account the different absorption behaviors of the two components. According to literature, there are five Raman active (A_{1g} + E_g + 3T_{2g}) modes in cubic spinel structure (space group Fd3m) [34]. NiFe₂O₄ ferrite is predominantly an inverse spinel. In general, the inverse spinel structure has the divalent cation occupying the octahedral sites and the trivalent cations are equally divided among the tetrahedral and remaining octahedral sites. In the NiFe₂O₄ spinel structure, the octahedral sites are occupied either by Ni or Fe ions [32]. All these five modes were observed at T_{2g} ~(189-212) cm⁻¹, E_g ~331 cm⁻¹, T_{2g} ~485 (NFO) cm⁻¹, T_{2g} ~530 (NFO) cm⁻¹, A_{1g} ~580 cm⁻¹ (NFO), A_{1g} ~702 (NFO) cm⁻¹ along with these modes, an additional vibrational modes at 449 cm⁻¹, A_{1g}(2) ~590 cm⁻¹, and at around 680 cm⁻¹ is also evidenced, which is attributed to the presence of Fe³⁺ on the A-site of AB₂O₄ [32]. These additional shoulders peaks correspond to the inverse spinel structure and stem from Ni²⁺ and Fe³⁺, which show an ordered arrangement on the octahedral site [32]. All the observed peaks are in complete agreement with earlier reports [32,35–37].

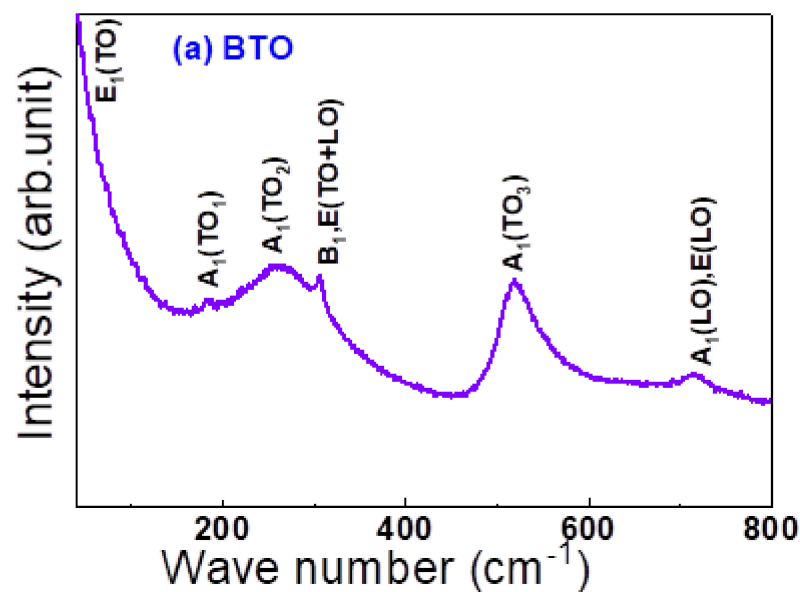


Figure 2. Cont.

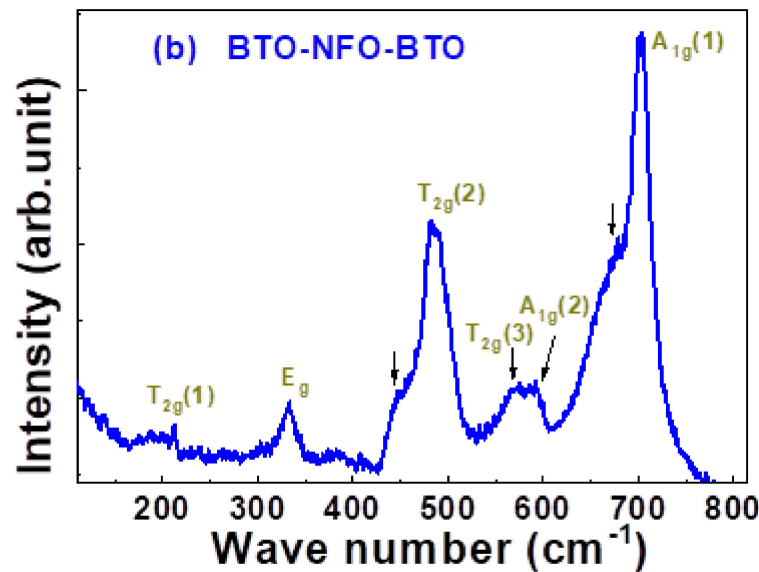


Figure 2. Raman Spectrum of the (a) BTO and (b) (BTO/NFO/BTO) tri-layered thin film at room temperature.

3.3. Surface Morphology Study

The surface morphology of (BTO/NFO/BTO) tri-layered thin film system was observed by SEM is displayed in Figure 3a. The SEM micrographs of film have shown uniform distribution of grains throughout the surface of the sample examined. The grains and grain boundaries are well defined in the sample. Dense microstructure in the (BTO/NFO/BTO) tri-layered system is attributed suitable annealing temperature of the PLD deposited films. The average grain size of (BTO/NFO/BTO) tri-layered films is about 50 nm as shown in the figure. Grain growth in these films might be due to higher annealing temperature ~ 700 °C. From the SEM micrograph (Figure 3a), (BTO/NFO/BTO) tri-layered films did not show any obvious agglomeration.

Cross-sectional SEM photographs exhibit microstructures of the Pt/BTO/NFO/BTO films deposited on Pt/TiO₂/SiO₂/Si substrates as shown in Figure 3b. The cross sectional image also shows a dense polycrystalline and smooth surface on trilayer heterostructure. Energy dispersive spectroscopy (EDX) measurements revealed presence of each element (Ba, Ti, Ni, Fe, and O, respectively) present in the tri-layered films (Figure 3c), and SEM-EDX shows all the elemental peaks of (BTO/NFO/BTO) tri-layered along with peaks corresponding to Pt/TiO₂/SiO₂/Si substrate.

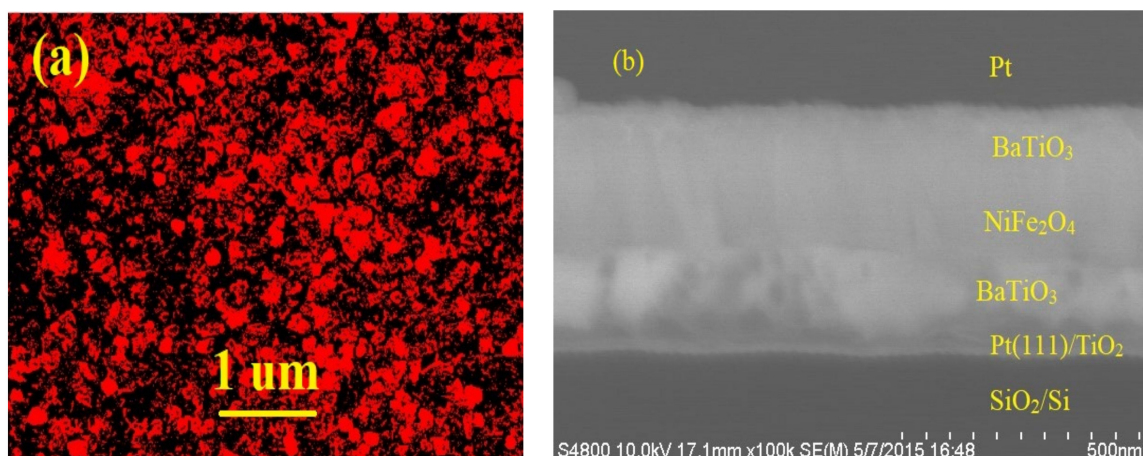


Figure 3. Cont.

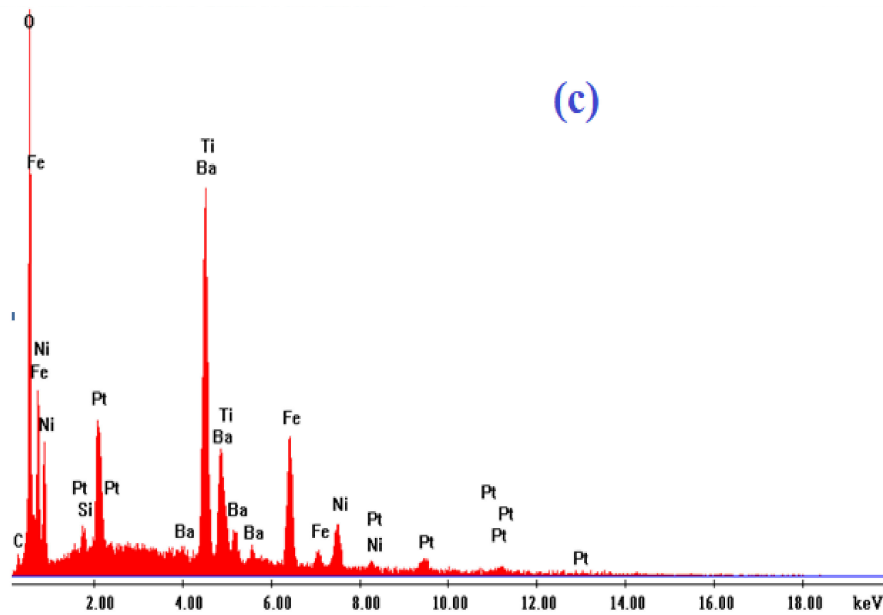


Figure 3. (a) Surface FE-SEM image. (b) Cross-sectional SEM image. (c) EDX image of the grown (BTO/NFO/BTO) tri-layered thin film on substrate Pt(111)/Ti/SiO₂/Si at room temperature.

3.4. Leakage Current Behavior

The leakage current density-external electric field characteristics (J - E) of a metal-insulator-metal (MIM) capacitor employing BTO-NFO-BTO tri-layered film is shown in Figure 4. Note from Figure 4 that there is an exponential increase of current with voltage at low voltages, followed by a saturation region at high voltages. The voltage-step and the delay-time after applying each voltage-step were fixed at 0.5 V and 1s, respectively in the log J versus E measurements. Relatively low leakage current density is observed for the tri-layered thin films. The films exhibit low leakage current density ($\sim 10^{-9}$ A/cm² at 0.3 MV/cm). Such reduction in leakage current density in these tri-layered films is correlated to higher annealing temperature (750 °C), and the completeness of perovskite phase formation in BTO-NFO-BTO films. At lower voltages, the leakage current is low and at high voltages the leakage current increases ($\sim 10^{-9}$ A/cm² at 0.1 MV/cm) to ($\sim 10^{-6}$ A/cm² at 0.3 MV/cm). The observed current density-electric field (J - V) loops are noticeably symmetrical in nature. The possible symmetry of the two branches in the leakage currents might be because the positive and negative biases were applied on single pad and both the top electrode and bottom electrode were of same in nature, rather than using different top and bottom electrode pads. Here, in this case, we have platinum (Pt) as both top and bottom electrodes. The J - E relationship curve in the region of low electric field, the MIM structure was found to follow an ohmic conduction mechanism ($J \propto E_n$, $n \sim 1$) [21,22]. Whereas, in the region of higher electric field, the observed behavior may be attributed to Schottky type conduction and space charge-limited current (SCLC) conduction model ($J \propto E_n$, $n > 1$) [23,24].

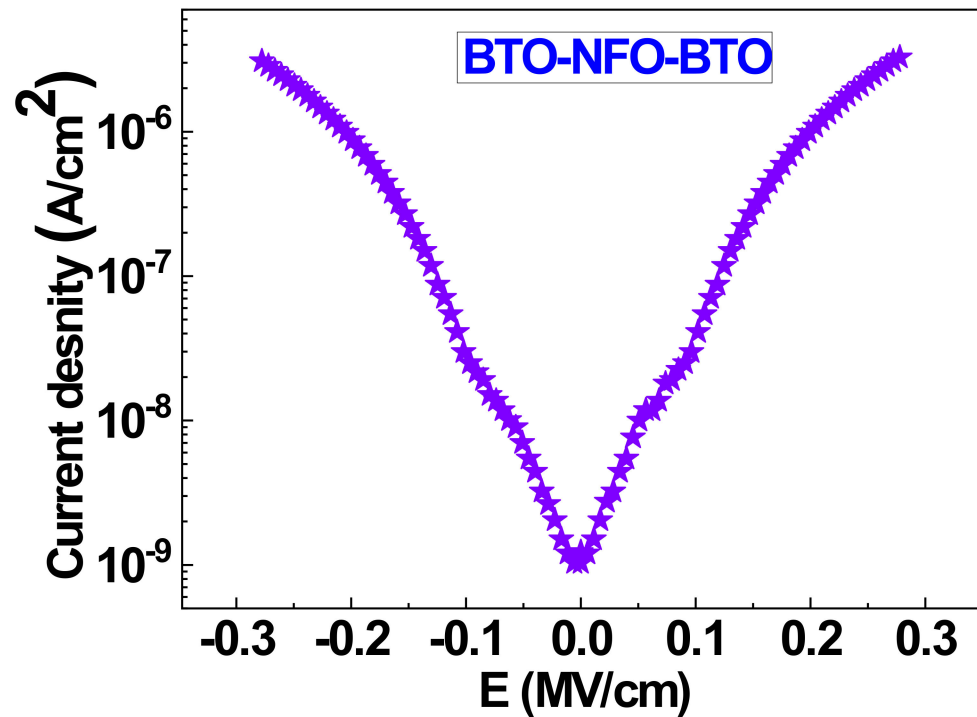


Figure 4. Leakage current behavior (current density versus voltage) of (BTO/NFO/BTO) tri-layered thin film on substrate Pt/Ti/SiO₂/Si at room temperature.

3.5. Dielectric Studies

Figure 5 shows the frequency dependent variation of dielectric constant (ϵ') and dielectric loss or loss tangent ($\text{Tan } \delta = (\epsilon')/(\epsilon'')$) of (BTO/NFO/BTO) thin film. The value of dielectric constant is found to decrease from 2145 (100 Hz) to 1414 (1 MHz) with increase in frequency. The dielectric constant (ϵ') decreased rapidly with the increase in frequency at room temperature. This decrease in dielectric constant attributed to the reduction of space charge polarization effect. Dielectric loss is a dielectric relaxation process, and it represents the energy loss of the capacitor which occurs when the polarization of capacitor shifts behind the applied electric field caused by the grain boundaries. In a capacitor, dielectric loss originates from either from space charge migration that is the interfacial polarization contribution or due to the movement of the molecular dipoles (dipole loss) and the direct current (DC) conduction mechanism [11,14,15]. Dielectric loss ($\text{tan } \delta$) increased with increase in frequency. The value of loss tangent value is found to be high (>0.25) in the region of high frequency region (1 MHz). At low frequency region tri-layered films have shown low dielectric loss (0.05). Dielectric properties have shown frequency dependence at room temperature. The high value of dielectric loss at a high frequency can be attributed to low resistivity of grain boundaries which is less effective than the grains [15].

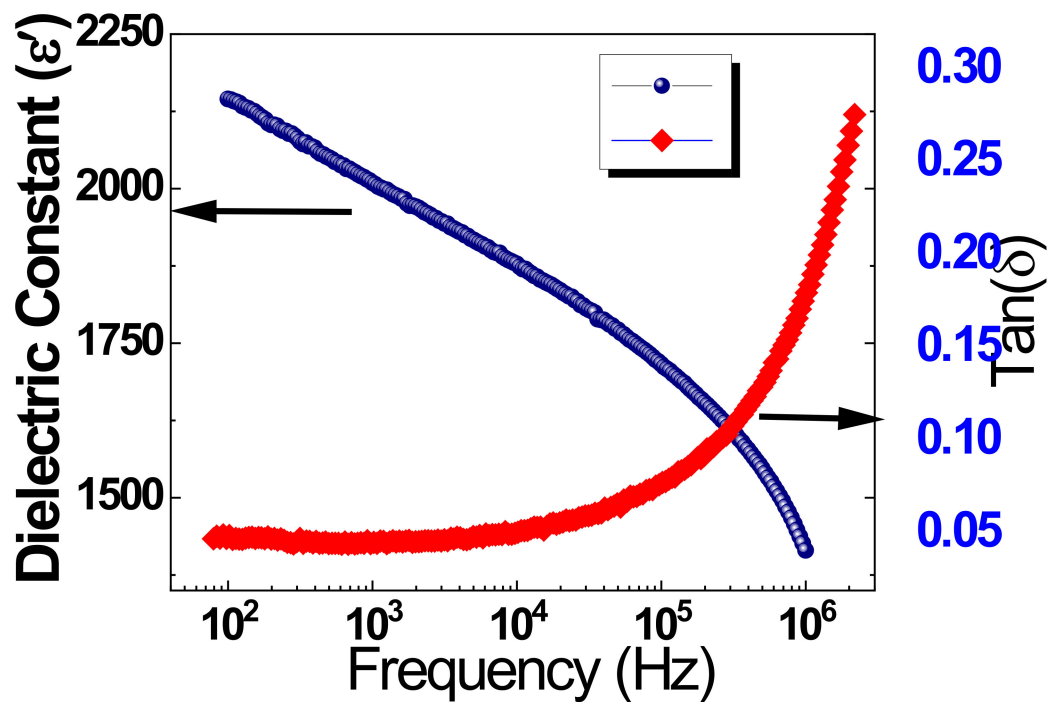


Figure 5. Room temperature dielectric properties (dielectric constant and dielectric loss-tan δ) of (BTO/NFO/BTO) tri-layered thin film on substrate Pt/Ti/SiO₂/Si.

3.6. Multiferroic Properties

To confirm the multiferroic properties of the (BTO/NFO/BTO) tri-layered thin films, we have measured the magnetization as a function of magnetic field and ferroelectric polarization as a function of electric field at room temperature.

3.6.1. M-H Hysteresis Curve

Figure 6 shows M-H hysteresis curve of the films deposited at 100 mTorr oxygen partial pressure. M-H hysteresis loops show a well-saturated ferromagnetic hysteretic behavior at room temperature. The magnetization curves present ferromagnetic ordering in NFO layers with a reasonably high saturation magnetization of ~ 16 emu/cm³ at room temperature. However, the observed value is less than the reported value of bulk NFO (~ 270 emu/cm³) [38]. The reduction in magnetization as compared to bulk NFO can be due to the small grain size of the films. The thermal energy in the samples has a significant effect on the magnetization. As the grain size decreases, thermal fluctuations increase, resulting in the reduction in magnetization. However, a higher magnetization (~ 78 emu/cm³) is recorded at 100 K. At low temperatures, the thermal energy is small so that the domains can easily be oriented along the applied field. Therefore, the increase in magnetization at low temperature can be attributed to the reorientation of the magnetic domains. The obtained saturation magnetization is comparable to the values previously reported in NFO-PZT heterostructures [26]. The coercivity of the sample is also found to increase when the temperature is decreased (from 130 Oe to 450 Oe). This too can be attributed to the reduction in thermal fluctuations.

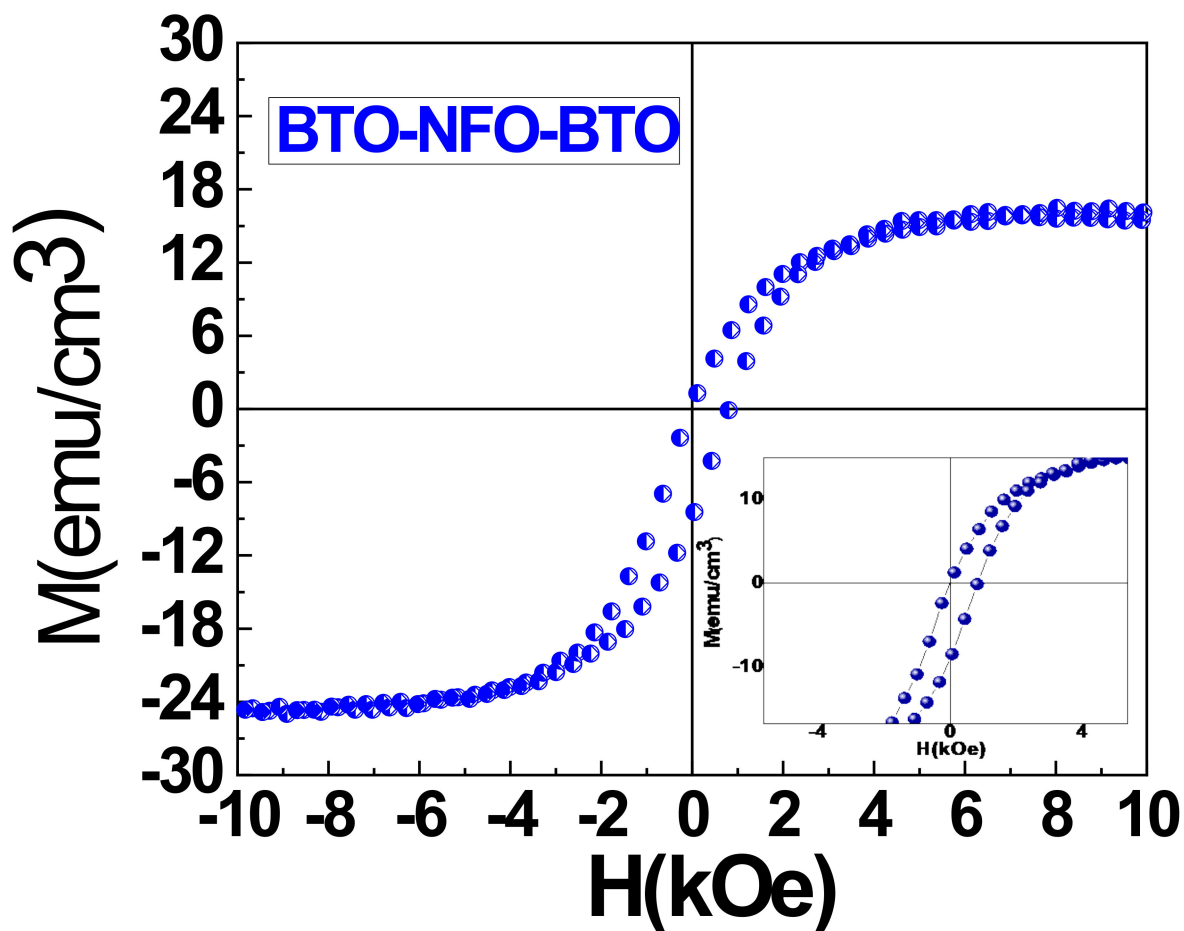


Figure 6. Magnetization-Electric Field Hysteresis loop of (BTO/NFO/BTO) tri-layered thin film deposited at room temperature.

3.6.2. P-E Hysteresis Curve

Figure 7 shows the variation of electrical polarization (P) with the applied electric field (E) at different dc electric fields of (BTO/NFO/BTO) tri-layered films at room temperature at fixed frequency of 1 kHz. From the P-E loops, it has been observed that, a complete saturation is not observed in P-E which might be due to the existence of leakage currents at very high fields in the samples. The coercive field and remnant polarization increase with increase of electric field. This behavior suggests the ferroelectric nature of the samples. The ferroelectric nature of (BTO/NFO/BTO) tri-layered is demonstrated by a hysteresis loop between polarization (P) and applied electric field (E) obtained at different selected voltages (5 V–20 V) as shown in Figure 7, and the P-E hysteresis loops were measured at room temperature to estimate the maximum/spontaneous polarization of present samples. P-E hysteresis loops were measured up to a maximum electric field of 0.25 MV/cm. It can be observed from the Figure that the remnant polarization value is found to be $10.82 \mu\text{Ccm}^{-2}$, while the maximum polarization value is equal to $15.75 \mu\text{Ccm}^{-2}$. As the electric field increased from 0.55 MV/cm to 2.08 MV/cm, both maximum (saturation) polarization (P_s) and the remnant polarization (P_r) were increased. From the hysteresis loops it is observed that as the voltage increases, the P-E loop becomes slanted. The tri-layered film (BTO/NFO/BTO) also shows a rather asymmetric hysteresis behavior. From P-E hysteresis loops, it is also visible that there is a gap in the negative polarization axis. The gap is real and is caused by temporary memory that decays away in a few seconds. Therefore, the origin of the discontinuity in the P-E ferroelectric hysteresis loops observed here may be due to the polarization relaxation [38,39]. Similar effect is also observed in some of the

reported on ferroelectric materials, where ferroelectric hysteresis loops exhibited such kind of discontinuity [38,39].

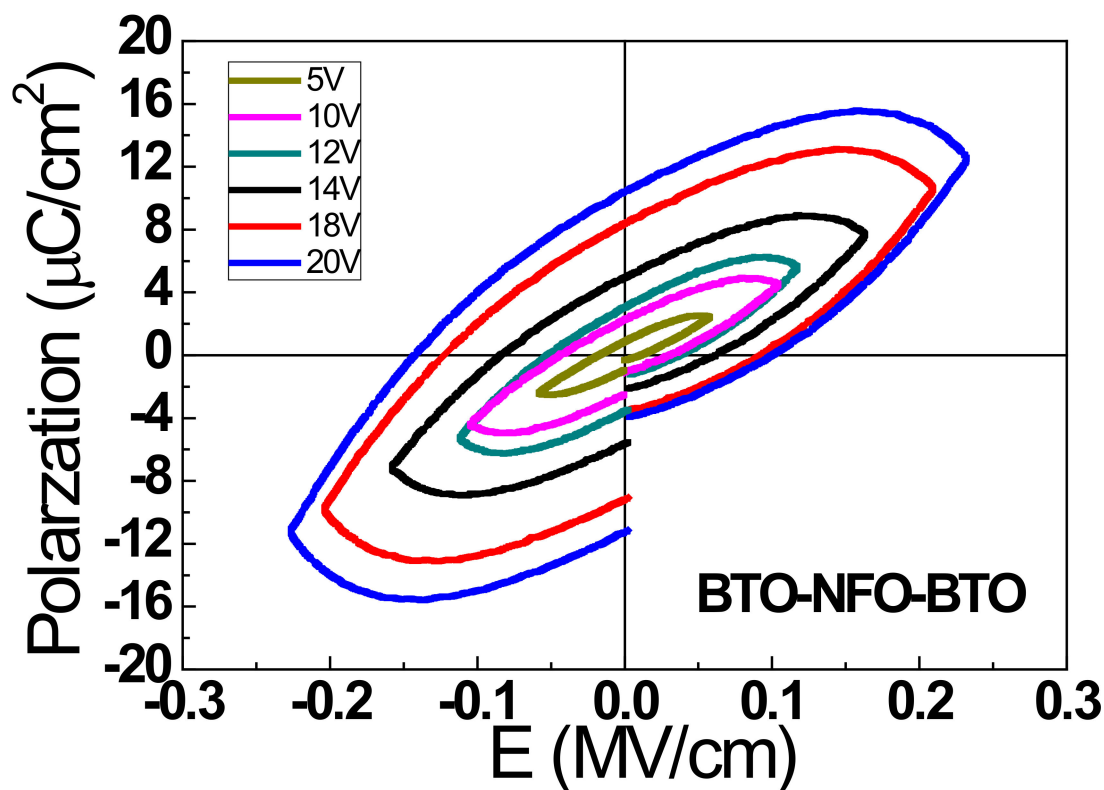


Figure 7. Polarization-Electric Field Hysteresis loop of (BTO/NFO/BTO) tri-layered thin film deposited at room temperature.

3.6.3. Magnetoelectric (ME) Coupling Effect

We performed the ME characterization by the dynamic method at room temperature. In the dynamic ME method, an ac magnetic field δH generated by a solenoid, was superimposed onto a DC bias magnetic field H_{bias} and both were applied parallel to the sample plane and the change in the voltage δV across the tri-layered films was measured. The electric field E induced by δH and H_{bias} was measured using a lock-in amplifier (SRS Inc., SR830). In the present case, the small alternating magnetic field $\delta H = 1$ Oe (at frequency of 1 kHz) was superimposed and DC bias magnetic field H_{bias} varied from 0 kOe to ± 3 kOe. The ME voltage coefficient (α_E) is defined as $\alpha_E = \delta E / \delta H = \delta V / (\delta H \times t)$, where δV is the measured output voltage, δH is the applied ac magnetic field and t is the total thickness of the ferroelectric phase in the composite thin film.

As discussed in the above sections, the coexistence of ferroelectric and ferromagnetic behaviors in these films is also attributed to the measurable ME effect. Magnetoelectric (ME) effect in tri-layered BTO/NFO/BTO thin films is shown in Figure 8. The variation of magnetoelectric voltage coefficient (α_E) with applied DC bias magnetic field (H_{bias}) is shown in figure. The (BTO/NFO/BTO) tri-layered thin films shows increase in α_E with H to a maximum of 54.5 mV/cm Oe, at 500 Oe bias field followed by a sharp decrease to 23.6 mV/cm Oe at bias field of +3 kOe. This kind of behavior was also reported in single phase multiferroics, thin films (polycrystalline/epitaxial), and bi- and multilayered composite structures [10,40–47]. From the figure, it is observed that α_E value does not decrease to zero value with increasing H . It is known that the ME voltage coefficients (α_E) is directly proportional to the product of the piezomagnetic coefficient $q = d\lambda/dH$ (where λ is the magnetostriction) and the piezoelectric coefficient. As the ME voltage arises due to magnetic–mechanical–electrical interactions, α_E is proportional to $q \times d$, its H_{dc} dependence is likely to follow the slope of λ vs H_{bias} of the magnetic material [45–48].

The magnetostriction of NFO is expected to be stronger at lower H in these heterostructures and decreases with increasing H . A similar type of magnetic field dependence of magnetostriction behavior of nickel ferrite has been reported [48]. In the present case, the increase or decrease of α_E with H_{bias} is not similar with the application of positive and negative magnetic field. This asymmetry in the ME coefficient attributed to the existence of magnetic anisotropy in this tri-layered films and clamping of bottom ferroelectric layer with electrode coated substrate.

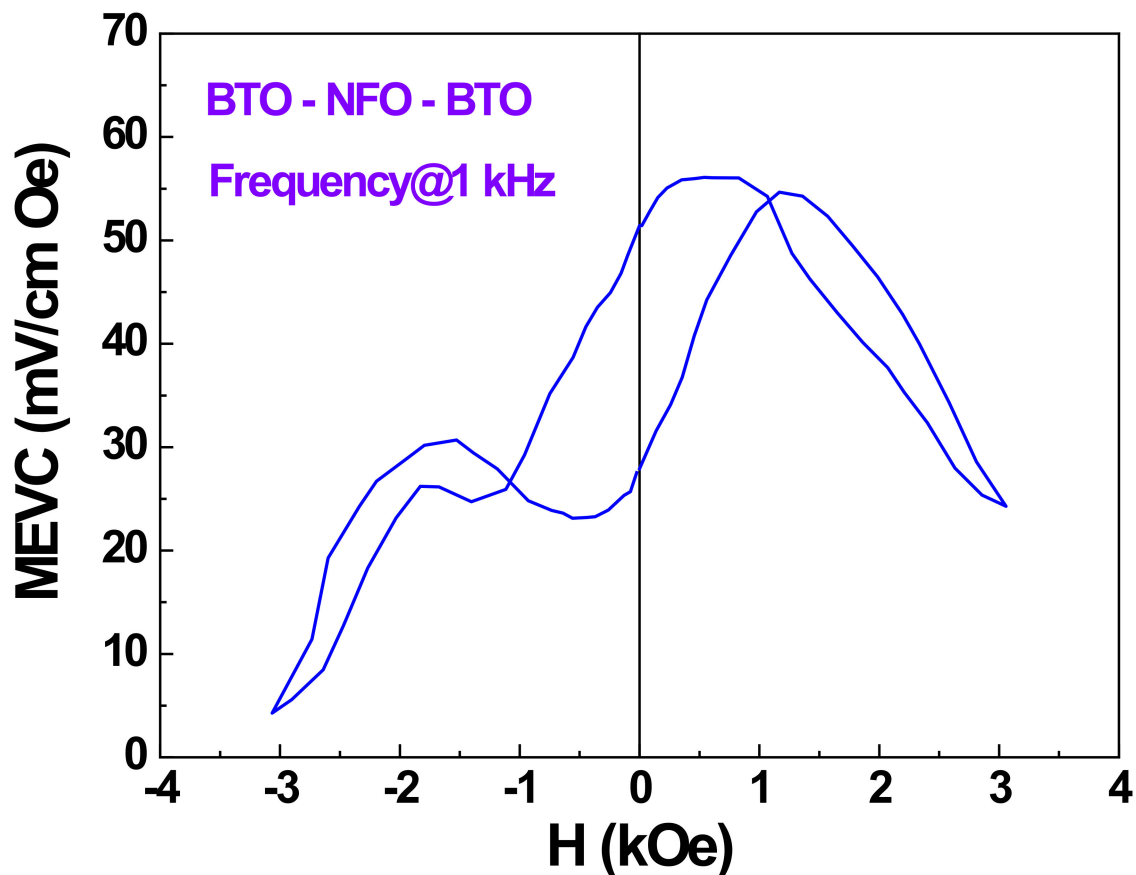


Figure 8. Magnetolectric (ME) effect in tri-layered BTO/NFO/BTO thin films.

Despite the observed ME coupling coefficient (α_E) ~ 54.5 mV/cm Oe, in our BTO/NFO/BTO tri-layer thin film, is significantly higher than NFO/BTO epitaxial bilayer hetero structures (12.1 mV/cmOe), BTO/NFO/BTO tri-layers (32 mV/cmOe) and BTO/NFO/BTO penta layers (36 mV/cmOe), $\text{Pb}(\text{Zr}_{0.4}\text{Ti}_{0.6})\text{O}_3\text{-Ni}_{0.8}\text{Zn}_{0.2}\text{Fe}_2\text{O}_4$ multilayered thin films (15 mV/cmOe), and comparable with $\text{BiFeO}_3/\text{BaTiO}_3$ bilayer (61 mV/cmOe) [43–48]. One can observe that even at H_{bias} equal to zero, the tri-layer composite film exhibits an initial high α_E value (i.e., 50 mV/cmOe) much larger than that of the bulk ferroelectric–ferromagnetic composite which is nearly close to zero. The zero-bias ME affect and the decrease in α_E upon reversal of H direction indicate the possible presence of a uniaxial “built-in” magnetic field in the film.

4. Conclusions

In summary, in the present work we have successfully deposited high quality polycrystalline multiferroic BTO/NFO/BTO tri-layered thin films using the pulsed laser deposition method on the technologically important substrate Pt(111)/TiO₂/SiO₂/Si substrate. At an optimized deposition temperature ~ 750 °C and oxygen partial pressure ~ 100 mTorr, tri-layered thin films have shown interesting multiferroic magnetolectric properties. The XRD patterns have shown complete stoichiometry transfer from bulk ceramic target to that

of films and showed no unwanted phase at the optimized growth temperature of 750 °C. These films have shown interesting ferroelectric properties with a maximum polarization of (~15.75 μCcm^{-2}) and a remnant polarization value of ~10.82 μCcm^{-2} at about a maximum electric field of 0.3 MV/cm. Ferromagnetic properties include a maximum magnetization of 16 emu/cm³ at ~10 kOe. These films also displayed low leakage current behavior at room temperature. It could be concluded that chemical composition controlled BTO/NFO/BTO thin films can be used to optimize the multiferroic Magnetoelectric properties. The acquired results are interesting for spintronic applications.

Author Contributions: V.S.P. designed, synthesized bulk materials and PLD thin films and characterized XRD, Raman, ferroelectric, ferromagnetic measurements of the samples. V.S.P. wrote the complete manuscript. D.K.P., helped in characterization dielectric, ferroelectric measurements. K.M. helped in SEM, EDX measurements. G.S., S.N.B., N.V.P. helped in getting ferromagnetic, ME coupling data. D.B.C. and R.S.K. supervised this research work. All authors have read and agreed to the published version of the manuscript.

Funding: The author, V.S.P. acknowledges National Research Council (NRC) senior research associate fellowship program. This work was supported in part by the Air Force Office of Scientific Research and by the Air Force Research Laboratory, Directed Energy Directorate.

Data Availability Statement: Not applicable.

Acknowledgments: The author, VSP acknowledges National Research Council (NRC) senior research associate fellowship program. This work was supported in part by the Air Force Office of Scientific Research and by the Air Force Research Laboratory, Directed Energy Directorate. R.S.K. acknowledges DoD Project #FA9550-20-1-0064.

Conflicts of Interest: The authors declare no conflict of interest.

References

1. Aizu, K. Possible species of ferromagnetic, ferroelectric, and ferroelastic crystals. *Phys. Rev. B* **1970**, *2*, 754. [[CrossRef](#)]
2. Hill, N.A. Why are there so few magnetic ferroelectrics? *J. Phys. Chem. B* **2000**, *104*, 6694–6709. [[CrossRef](#)]
3. Scott, J.F. Room-temperature multiferroic magnetoelectrics. *NPG Asia Mater.* **2013**, *5*, e72. [[CrossRef](#)]
4. dos Santos, A.M.; Parashar, S.; Raju, A.R.; Zhao, Y.S.; Cheetham, A.K.; Rao, C.N.R. Evidence for the likely occurrence of magnetoferroelectricity in the simple perovskite, BiMnO₃. *Solid State Commun.* **2002**, *122*, 49–52. [[CrossRef](#)]
5. Wang, J.; Zhang, Y.; Ma, J.; Lin, Y.; Nan, C.W. Magnetoelectric behavior of BaTiO₃ films directly grown on CoFe₂O₄ ceramics. *J. Appl. Phys.* **2008**, *104*, 014101. [[CrossRef](#)]
6. Fiebig, M.; Lottermoser, T.; Fröhlich, D.; Goltsev, A.V.; Pisarev, R.V. Observation of coupled magnetic and electric domains. *Nature* **2002**, *419*, 818–820. [[CrossRef](#)] [[PubMed](#)]
7. Laletsin, U.; Padubnaya, N.; Srinivasan, G.; Devreugd, C.P. Frequency dependence of magnetoelectric interactions in layered structures of ferromagnetic alloys and piezoelectric oxides. *Appl. Phys. A* **2004**, *78*, 33–36. [[CrossRef](#)]
8. Jia, T.; Cheng, Z.; Zhao, H.; Kimura, H. Domain switching in single-phase multiferroics. *Appl. Phys. Rev.* **2018**, *5*, 021102. [[CrossRef](#)]
9. Palkar, V.R.; John, J.; Pinto, R. Observation of saturated polarization and dielectric anomaly in magnetoelectric BiFeO₃ thin films. *Appl. Phys. Lett.* **2002**, *80*, 1628–1630. [[CrossRef](#)]
10. Wang, J.; Neaton, J.B.; Zheng, H.; Nagarajan, V.; Ogale, S.B.; Liu, B.; Viehland, D.; Vaithyanathan, V.; Schlom, D.G.; Waghmare, U.V.; et al. Epitaxial BiFeO₃ Multiferroic Thin Film Heterostructures. *Science* **2003**, *299*, 1719–1722. [[CrossRef](#)]
11. Puli, V.S.; Pradhan, D.K.; Katiyar, R.K.; Coondoo, I.; Panwar, N.; Misra, P.; Chrisey, D.B.; Scott, J.F.; Katiyar, R.S. Photovoltaic effect in transition metal modified polycrystalline BiFeO₃ thin films. *J. Phys. D Appl. Phys.* **2014**, *47*, 075502. [[CrossRef](#)]
12. Lente, M.H.; Guerra, J.D.S.; de Souza, G.K.S.; Fraygola, B.M.; Raigoza, C.F.V.; Garcia, D.; Eiras, J.A. Nature of the magnetoelectric coupling in multiferroic Pb(Fe_{1/2}Nb_{1/2})O₃ ceramics. *Phys. Rev. B* **2008**, *78*, 054109. [[CrossRef](#)]
13. Kleemann, W.; Shvartsman, V.; Borisov, P.; Kania, A. Coexistence of Antiferromagnetic and Spin Cluster Glass Order in the Magnetoelectric Relaxor Multiferroic PbFe_{0.5}Nb_{0.5}O₃. *Phys. Rev. Lett.* **2010**, *105*, 257202. [[CrossRef](#)]
14. Pradhan, D.K.; Sahoo, S.; Barik, S.K.; Puli, V.S.; Misra, P.; Katiyar, R.S. Studies on magnetoelectric coupling in PFN-NZFO composite at room temperature. *J. Appl. Phys.* **2014**, *115*, 194105. [[CrossRef](#)]
15. Pradhan, D.K.; Kumari, S.; Vasudevan, R.K.; Dugu, S.; Das, P.T.; Puli, V.S.; Pradhan, D.K.; Kalinin, S.V.; Katiyar, R.S.; Rack, P.D.; et al. Room temperature multiferroicity and magnetodielectric coupling in 0–3 composite thin films. *J. Appl. Phys.* **2020**, *127*, 194104. [[CrossRef](#)]

16. da Silveira Lacerda, L.H.; Ribeiro, R.A.P.; Lazaro, S.R. Magnetic, electronic, ferroelectric, structural and topological analysis of AlFeO_3 , FeAlO_3 , FeVO_3 , BiFeO_3 and PbFeO_3 materials: Theoretical evidences of magnetoelectric coupling. *J. Magn. Magn. Mater.* **2019**, *480*, 199–208. [CrossRef]
17. Li, Y.; Wang, Y.G.; Wang, N.; Wang, F.L.; Jain, A. Magnetoelectric $(1-x)\text{AlFeO}_3$ - $x\text{BaTiO}_3$ solid solutions with ferroelectric relaxor behavior near room temperature. *Ceram. Int.* **2020**, *46*, 7930–7938. [CrossRef]
18. Shastry, S.; Srinivasan, G.; Bichurin, M.I.; Petrov, V.M.; Tatarenko, A.S. Microwave magnetoelectric effects in single crystal bilayers of yttrium iron garnet and lead magnesium niobate-lead titanate. *Phys. Rev. B* **2004**, *70*, 064416. [CrossRef]
19. Zheng, H.; Wang, J.; Lofland, S.E.; Ma, Z.; Mohaddes-Ardabili, L.; Zhao, T.; Salamanca-Riba, L.; Shinde, S.R.; Ogale, S.B.; Bai, F.; et al. Multiferroic BaTiO_3 - CoFe_2O_4 nanostructures. *Science* **2004**, *303*, 661–663. [CrossRef] [PubMed]
20. Pradhan, D.K.; Kumari, S.; Vasudevan, R.K.; Strelcov, E.; Puli, V.S.; Pradhan, D.K.; Kumar, A.; Gregg, J.M.; Pradhan, A.K.; Kalinin, S.V.; et al. Exploring the Magnetoelectric Coupling at the Composite Interfaces of FE/FM/FE Heterostructures. *Sci. Rep.* **2018**, *8*, 17381. [CrossRef]
21. Moreira dos Santos, A.; Cheetham, A.K.; Atou, T.; Syono, Y.; Yamaguchi, Y.; Ohoyama, K.; Chiba, H.; Rao, C.N.R. Orbital ordering as the determinant for ferromagnetism in biferroic BiMnO_3 . *Phys. Rev. B* **2002**, *66*, 064425. [CrossRef]
22. Puli, V.S.; Pradhan, D.K.; Gollapudi, S.; Coondoo, I.; Panwar, N.; Adireddy, S.; Chrisey, D.B.; Katiyar, R.S. Magnetoelectric coupling effect in transition metal modified polycrystalline BiFeO_3 thin films. *J. Magn. Magn. Mater.* **2014**, *369*, 9–13. [CrossRef]
23. Panwar, N.; Coondoo, I.; Tomar, A.; Kholkin, A.L.; Puli, V.S.; Katiyar, R.S. Nanoscale piezoresponse and magnetic studies of multiferroic Co and Pr co-substituted BFO thin films. *Mater. Res. Bull.* **2012**, *47*, 4240–4245. [CrossRef]
24. Choi, T.; Horibe, Y.; Yi, H.T.; Choi, Y.J.; Wu, W.D.; Cheong, S.W. Insulating interlocked ferroelectric and structural antiphase domain walls in multiferroic YMnO_3 . *Nat. Mater.* **2010**, *9*, 253–258. [CrossRef]
25. Jang, S.Y.; Lee, D.; Lee, J.-H.; Murugavel, P.; Chung, J.-S.; Jin-Seok, C.; Yup, J.S.; Daesu, L.; Jung-Hyuk, L.; Pattukkannu, M. Ferroelectric Properties of Multiferroic Hexagonal ErMnO_3 Thin Films. *J. Korean Phys. Soc.* **2009**, *55*, 841–845. [CrossRef]
26. Kimura, T.; Goto, T.; Shintani, H.; Ishizaka, K.; Arima, T.; Tokura, Y. Magnetic control of ferroelectric polarization. *Nature* **2003**, *426*, 55–58. [CrossRef]
27. Zhao, H.Y.; Kimura, H.; Cheng, Z.X.; Osada, M.; Wang, J.L.; Wang, X.L.; Dou, S.X.; Liu, Y.; Yu, J.D.; Matsumoto, T.; et al. Large magnetoelectric coupling in magnetically short-range ordered $\text{Bi}_5\text{Ti}_3\text{FeO}_{15}$ film. *Sci. Rep.* **2014**, *4*, 5255. [CrossRef] [PubMed]
28. Imai, A.; Cheng, X.; Xin, H.L.; Eliseev, E.A.; Morozovska, A.N.; Kalinin, S.V.; Takahashi, R.; Lippmaa, M.; Matsumoto, Y.; Nagarajan, V. Epitaxial $\text{Bi}_5\text{Ti}_3\text{FeO}_{15}$ - CoFe_2O_4 pillar-matrix multiferroic nanostructures. *ACS Nano* **2013**, *7*, 11079–11086. [CrossRef] [PubMed]
29. Sepelak, V.; Baabe, D.; Mienert, D.; Schultze, D.; Krumeich, F.; Litterst, F.J.; Becker, K.D. Evolution of structure and magnetic properties with annealing temperature in nanoscale high-energy-milled nickel ferrite. *J. Magn. Magn. Mater.* **2003**, *257*, 377–386. [CrossRef]
30. Powder Diffraction File, Joint Committee on Powder Diffraction Standards. International Centre for Diffraction Data, Cards. 2004, 10-325 and 5-626. Available online: <https://www.icdd.com/pdfsearch/> (accessed on 31 August 2021).
31. Gonçalves, J.R.; Barbosa, J.; Sá, P.; Mendes, J.A.; Rolo, A.G.; Almeida, B.G. Structural and Raman characterization of nanogranular BaTiO_3 - NiFe_2O_4 thin films deposited by laser ablation on Si/Pt substrates. *Phys. Status Solidi C* **2010**, *7*, 2720–2723. [CrossRef]
32. Ahlawat, A.; Sathe, V.G. Raman study of NiFe_2O_4 nanoparticles, bulk and films: Effect of laser power. *J. Raman Spectrosc.* **2011**, *42*, 1087–1094. [CrossRef]
33. Puli, V.S.; Pradhan, D.K.; Riggs, B.C.; Adireddy, S.; Katiyar, R.S.; Chrisey, D.B. Synthesis and characterization of lead-free ternary component BST-BCT-BZT ceramic capacitors. *J. Adv. Dielectr.* **2014**, *4*, 1450014. [CrossRef]
34. Puli, V.S.; Li, P.; Adireddy, S.; Chrisey, D.B. Crystal structure, dielectric, ferroelectric and energy storage properties of La-doped BaTiO_3 semiconducting ceramics. *J. Adv. Dielectr.* **2015**, *5*, 1550027. [CrossRef]
35. Iliev, M.N.; Mazumdar, D.; Ma, J.X.; Gupta, A.; Rigato, F.; Fontcuberta, J. Monitoring B-site ordering and strain relaxation in NiFe_2O_4 epitaxial films by polarized Raman spectroscopy. *Phys. Rev. B* **2011**, *83*, 014108. [CrossRef]
36. Chandramohan, P.; Srinivasan, M.P.; Velmurugan, S.; Narasimhan, S.V. Cation distribution and particle size effect on Raman spectrum of CoFe_2O_4 . *J. Solid State Chem.* **2011**, *184*, 89–96. [CrossRef]
37. Quandt, N.; Roth, R.; Syrowatka, F.; Steimecke, M.; Ebbinghaus, S.G. Spin-Coating and Characterization of Multiferroic MFe_2O_4 ($\text{M}=\text{Co}, \text{Ni}$)/ BaTiO_3 Bilayers. *J. Solid State Chem.* **2016**, *233*, 82–89. [CrossRef]
38. Puli, V.S.; Pradhan, D.K.; Adireddy, S.; Martínez, R.V.; Silwal, P.; Scott, J.F.; Ramana, C.V.; Chrisey, D.B.; Katiyar, R.S. Nanoscale polarisation switching and leakage currents in $(\text{Ba}_{0.955}\text{Ca}_{0.045})(\text{Zr}_{0.17}\text{Ti}_{0.83})\text{O}_3$ epitaxial thin films. *J. Phys. D Appl. Phys.* **2015**, *48*, 355502. [CrossRef]
39. Puli, V.S.; Pradhan, D.K.; Coondoo, I.; Panwar, N.; Adireddy, S.; Luo, S.; Katiyar, R.S.; Chrisey, D.B. Observation of Large enhancement in energy-storage properties of lead-free polycrystalline $0.5\text{BaZr}_{0.2}\text{Ti}_{0.8}\text{O}_3$ - $0.5\text{Ba}_{0.7}\text{Ca}_{0.3}\text{TiO}_3$ ferroelectric thin films. *J. Phys. D Appl. Phys.* **2019**, *52*, 255304. [CrossRef]
40. Kumari, S.; Kimura, H.; Cheng, Z.; Osada, M.; Wang, J.; Wang, X.; Dou, S.X.; Liu, Y.; Yu, J.; Matsumoto, T.; et al. Dielectric Anomalies Due to Grain Boundary Conduction in Chemically Substituted BiFeO_3 . *J. Appl. Phys.* **2015**, *117*, 114102. [CrossRef]
41. Cheng, Z.X.; Wang, X.L.; Zhao, H.Y.; Kimura, H. Lead-free potassium bismuth titanate thin film with complex Aurivillius layer structure. *J. Appl. Phys.* **2010**, *107*, 084105. [CrossRef]

42. Deng, C.; Zhang, Y.; Ma, J.; Lin, Y.; Nan, C.-W. Magnetic-electric properties of epitaxial multiferroic NiFe₂O₄—BaTiO₃ heterostructure. *J. Appl. Phys.* **2007**, *102*, 074114. [[CrossRef](#)]
43. Liu, J.; Zhang, Y.; Lin, Y.; Nan, C.-W. Magnetoelectric coupling in BaTiO₃/(NiFe₂O₄/BaTiO₃)_n (n = 1, 2, 3, 4) multilayered thin films. *J. Appl. Phys.* **2009**, *105*, 083915. [[CrossRef](#)]
44. Ryu, S.; Park, J.H.; Jang, H.M. Magnetoelectric coupling of [00l]-oriented Pb (Zr_{0.4}Ti_{0.6})O₃—Ni_{0.8}Zn_{0.2}Fe₂O₄ multilayered thin films. *Appl. Phys. Lett.* **2007**, *91*, 142910. [[CrossRef](#)]
45. Gupta, R.; Chaudhary, S.; Kotnala, R.K. Interfacial Charge Induced Magnetoelectric Coupling at BiFeO₃/BaTiO₃ Bilayer Interface. *ACS Appl. Mater. Interfaces* **2015**, *7*, 8472–8479. [[CrossRef](#)] [[PubMed](#)]
46. Ma, J.; Hu, J.; Li, Z.; Nan, C.-W. Recent Progress in Multiferroic Magnetoelectric Composites: From Bulk to Thin Films. *Adv. Mater.* **2011**, *23*, 1062–1087. [[CrossRef](#)] [[PubMed](#)]
47. Vaz, C.A.F.; Hoffman, J.; Ahn, C.H.; Ramesh, R. Magnetoelectric Coupling Effects in Multiferroic Complex Oxide Composite Structures. *Adv. Mater.* **2010**, *22*, 2900–2918. [[CrossRef](#)]
48. Srinivasan, G.; Rasmussen, E.T.; Gallegos, J.; Bokhan, Y.I.; Laletin, V.M. Magnetoelectric bilayer and multilayer structures of magnetostrictive and piezoelectric oxides. *Phys. Rev. B* **2001**, *64*, 214408. [[CrossRef](#)]